Millimeter-wave Backscatter: A Quantum Leap for Gigabit Communication, RF Sensing, and Wearables

John Kimionis
School of Electrical and Computer Engineering
Georgia Institute of Technology
Atlanta, GA 30308
Email: ikimionis@gatech.edu

Apostolos Georgiadis
School of Engineering and Physical Sciences
Heriot-Watt University
Edinburgh EH14 4AS, Scotland, UK
Email: a.georgiadis@hw.ac.uk

Manos M. Tentzeris
School of Electrical and Computer Engineering
Georgia Institute of Technology
Atlanta, GA 30308
Email: etentze@ece.gatech.edu

***Abstract*—The first-ever reported Gbps backscatter transmission is presented at millimeter-wave frequencies, extremely expanding the potential of backscatter radio as a low-energy, low-complexity communication platform. Minimal front-ends are implemented that can be used for multi-gigabit communication and RF sensing, achieving scattering frequencies of at least 4 GHz away from a carrier center frequency of 24 GHz. The significantly wideband operation of these minimal communicators will enable broadband wireless transmission with less than 0.15 pJ/bit front-end energy consumption at 4 Gbps and sensing with an extensive number of low-power sensors. The front-ends are additively manufactured using inkjet printing on flexible substrates that can be directly integrated with wearables for challenging mobile applications in 5G and the Internet of Things (IoT).**

***Index Terms*—backscatter radio, millimeter-wave, 5G, Gbps, Internet of Things (IoT), flexible printed electronics, wearable RF sensors.**

I. Introduction

Backscatter radio has been increasingly used as a low-power and low-cost implementation of wireless communication, that can greatly benefit sensor networks. Most backscatter radio implementations in the literature are targeted for 2.4 GHz, 900 MHz, or lower frequencies (e.g. UHF) [1], [2], [3]. Although design at these frequency bands is favorable because of low transmission line and active component losses, higher frequencies on the millimeter-wave (mmWave) bands can offer extensive bandwidths which can extremely boost the transmission data rates.

This work demonstrates the design of an end-to-end mmWave backscatter system for communication and sensing, operating in the 24–28 GHz band. In this band, miniaturized high-gain antennas and antenna arrays can be implemented, in contrast with UHF bands, where antenna arrays can become bulky and impractical. The miniaturization that is possible in mmWave bands allows for system implementation with additive manufacturing technologies (AMTs) and direct integration with wearable and flexible electronics for mobile health, sensing, security, and short-range ultra high-speed data transmission. To achieve broadband data transmission, we leverage the backscattering operation to reflect subcarrier signals of GHz-level frequencies, which will enable multi-gigabit communication with single transistor front-ends and pJ/bit energy consumption. Typical digital backscatter/RFID systems at UHF frequency bands achieve kbps-level communication [4], [5], while high order constellation [6] and spectrally-efficient [7] tag front-ends can boost backscatter communication to Mbps-level datarates. With the proof-of-concept presented in this work, a quantum leap is made: multi-GHz bandwidth transmissions are possible at mmWave bands, allowing tags to perform complex *ultra wideband modulation*, such as orthogonal frequency-division multiplexing (OFDM), and achieving Gbit-level backscatter communication for the first time.

II. System Description

The mmWave backscatter system consists of a communicator and a custom reader front-end. The backscatter communicator/tag consists of a common-source low-power enhancement P-HEMT transistor (Avago VMMK-1225) that is directly interfaced to a circularly-polarized antenna array through its drain (Fig. 1) while its gate is biased with a positive voltage. The voltage pulses applied to the gate modulate the transistor's channel width and effectively modify the reflection coefficient

$$\Gamma = \frac{Z_d - Z_a^*}{Z_d + Z_a}, \tag{1}$$

where Z_t is the input impedance of the transistor at the drain terminal and Z_a is the antenna array's input impedance. The custom reader front-end consists of a voltage-controlled oscillator (VCO - Hittite HMC739) that generates a 24-GHz continuous wave (CW) that is amplified (PA - Hittite HMC863) and radiated through a linearly-polarized transmit (Tx) horn antenna. The receive chain of the measurement setup consists of a receive (Rx) antenna that is cross-polarized with respect to the Tx antenna to a) achieve Tx/Rx isolation and b) reject structural scattering from the backscatter tag's ground plane. The received signals are amplified with a low-noise amplifier (LNA) stage and are directly down-converted to DC with a zero-intermediate frequency (IF) mixer (Hittite HMC977). The baseband in-phase (I) and quadrature (Q) signals are routed to the inputs of a software defined radio (SDR - Ettus USRP N210) or a spectrum analyzer for digital processing and visualization.

978-1-5090-6360-4/17/$31.00 ©2017 IEEE

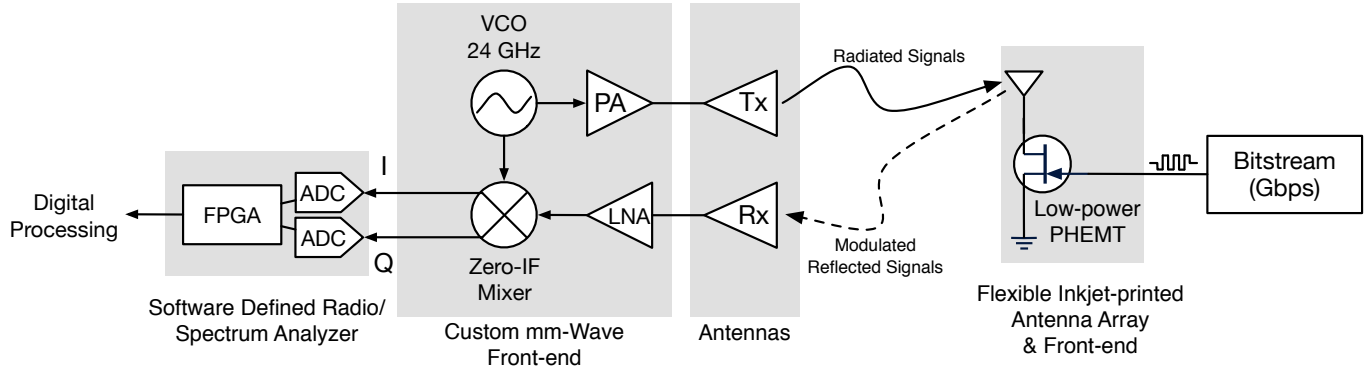

Fig. 1. End-to-end millimeter-wave backscatter system for Gigabit communication.

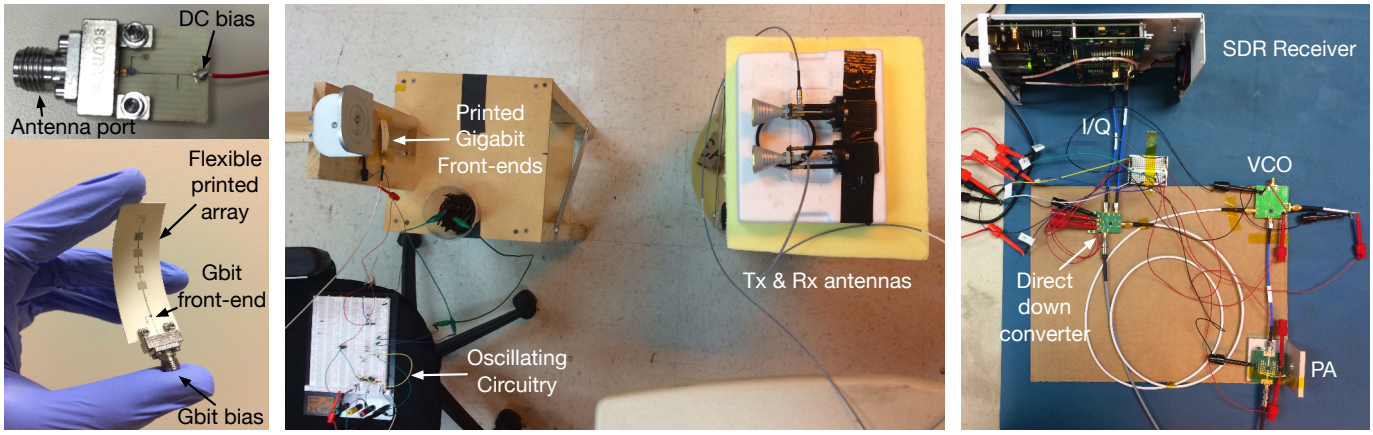

Fig. 2. Left: mm-wave backscatter front-end for characterization and flexible printed $\times$ 1 circularly-polarized antenna array with Gbit front-end. Center: Wireless measurement setup. Right: Tx and Rx chains with Software Defined Radio.

III. Measurements and Applications

A single-transistor front-end has been fabricated on a thin Rogers RO4003C laminate for wired characterization (Fig. 2-left) with a vector network analyzer (VNA). The PHEMT is biased through a microstrip-stub RF choke (rejection better than 25 dB at 24 GHz) and for a bias voltage of 0 V and 1 V respectively, the reflection coefficient values Γ_0 and Γ_1 are measured up to 40 GHz. Then, the reflection coefficient difference amplitude $|\Delta\Gamma| \triangleq |\Gamma_1 - \Gamma_0|$ is calculated, which is known as the modulation factor that needs to be maximized to optimize backscatter communication performance [8]. The measured $|\Delta\Gamma|$ shows a wideband operation around the 24-GHz band, where it remains within 0.9 to 1.2 between 23 and 28 GHz (Fig. 3).

The front-end is interfaced with a 5×1 circularly-polarized patch antenna array (up to 10 dBi gain) and the integrated system is manufactured on 7 mil flexible liquid crystal polymer (LCP) substrate ($\epsilon_r = 3.14, \tan\delta = 0.002$) with inkjet-printed silver nanoparticle (SNP) ink (conductivity $\sigma = 5 \times 10^6$ S/m) traces and conductive epoxy adhesive for placing the discrete PHEMT on the flexible board. An end-launch SMA RF connector is used for the bias port instead of a DC wire with high inductance, to support GHz-signal transistor biasing. The total board has a length of less than 7 cm and is completely

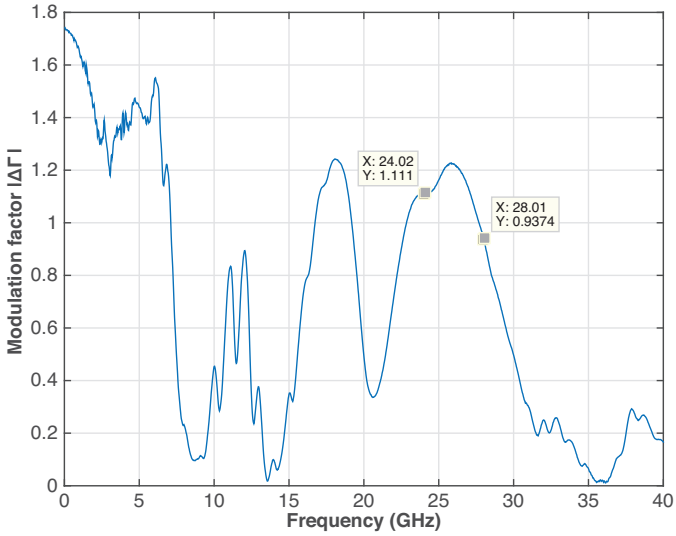

Fig. 3. Backscatter modulation factor $\Delta\Gamma$ versus frequency for front-end DC bias voltages of 0 V and 1 V.

978-1-5090-6360-4/17/$31.00 ©2017 IEEE

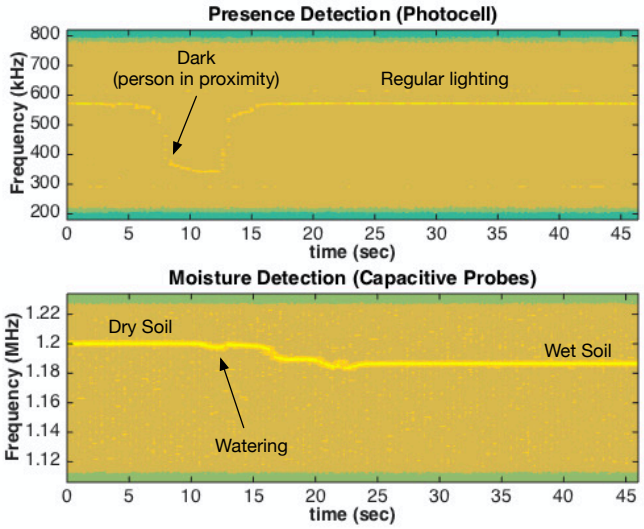

Fig. 4. Backscattered frequency for sensing examples. Top: Presence detection with photocell. Bottom: Soil moisture detection with capacitive probes.

flexible, with excellent silver ink adhesion (no conductor cracks while flexing), which makes it suitable for wearable-electronics integration, e.g. in conformal wristbands (Fig. 2-left).

The wireless measurement setup of Fig. 2-center has been used with the Tx/Rx chain of Fig. 2-right to test the operation of the mmWave backscatter tag in sensing and wideband communication scenarios. A low-voltage oscillating circuit based on a 555 timer integrated circuit (IC) has been prototyped as a generic interface for resistive and capacitive sensors. The circuit's output is a variable-frequency pulse-train that drives the PHEMT's gate and switches the transistor on and off with a frequency F_{sub} defined by the sensors' resistance or capacitance. When a CW carrier F_c illuminates the tag's antenna, a subcarrier of frequency F_c+F_{sub} is reflected towards the receiver, which can decode the sensor's information. As an example, a presence detection sensor with a resistive photocell has been implemented, that backscatters frequencies $F_{\text{sub}} = 600$ kHz away from the $F_c = 24$ GHz carrier in regular room lighting conditions, and around 350 kHz away, when a person is in proximity and interferes with the sensor's illumination. Also, a simple soil moisture sensor is implemented with probes whose capacitance increases when the soil is wet, and backscatters subcarriers 1.20 MHz and 1.18 MHz away from the 24-GHz carrier for dry and wet conditions, respectively. The received backscattered frequencies are shown in Fig. 4, where an operation similar to state-of-the-art backscatter oscillating sensors (e.g. [9]) can be seen.

The full potential of the implemented front-end is tested by biasing the tag with ultra high frequency subcarriers up to 5 GHz, in sharp contrast with the kHz–MHz-range subcarriers that are commonly used for backscatter tags in the UHF bands. Multiple tests have been conducted with ranges over 2 meters in indoor, cluttered environments and discrete frequency biasing around 500 MHz, 1 GHz, 2 GHz, 3 GHz, 4 GHz, and 5 GHz. The received subcarriers around the frequencies of 2 GHz and 4 GHz can be clearly seen in Fig. 5, 20–30 dB above the noise floor. A signal-to-noise ratio (SNR) estimate of the maximum versus the average channel power can be seen in Fig. 5-bottom, where it is apparent that a high-SNR, wideband operation can be achieved up to 4 GHz. This graph includes the *complete, compound* response of the *end-to-end system*, including the front-end's $|\Delta\Gamma|$ bandwidth, the printed antenna array's bandwidth, Tx chain VCO and PA efficiency, as well as Rx chain LNA and mixer bandwidth. The lower subcarrier SNR close to the 500 MHz frequency is due to the fact that clutter attributed to system nonlinearities, intermodulation products, low-frequency ambient scatterers, and phase noise increase while approaching the DC frequency, which is a known phenomenon in backscatter/RFID systems [2]. Nevertheless, the system shows an achievable end-to-end bandwidth of at least 4 GHz, which can enable dramatically-higher data rates, compared to the prior art, up to the Gbps-range.

To demonstrate the proof-of-concept of broadband backscatter communications, a bias frequency sweep has been performed from 1.5 GHz to 1.515 GHz, resulting in a backscattered spectrum from 25.5 GHz to 25.515 GHz. Although the bias frequency sweep can be performed for the full 0–4 GHz frequency range as shown in Fig. 5 (with backscatter from 24 to 28 GHz), a narrower sweep is shown for easy visualization in Fig. 6. It can be seen that the received backscattered spectrum resembles that of OFDM transmissions, widely used in WLAN and LTE systems. Equal-power, equally-spaced subcarriers form a rectangular-shaped spectral envelope of high SNR with respect to the noise floor, with each subcarrier modulated individually, resulting in high aggregate data rates. Most importantly, at subcarrier frequencies of 4 GHz and maximum biasing of 1 V, the front-end's static and dynamic (switching) power consumption are 200 nW and 0.6 mW, respectively, reaching an ultra-low energy-per-bit of less than $E_b = 0.15$ pJ/bit at 4 Gbps binary modulation (transistor on/off). It has to be mentioned that in OFDM, each subcarrier frequency can be loaded with a higher-order modulation scheme (e.g. quadrature amplitude modulation (QAM) [6]) which will result in multi-gigabit transmission rates from backscatter tags and will boost their potential as low-energy communicators for 5G and IoT networks.

IV. Conclusion, Vision, and Future Work

This work has demonstrated for the first time the mechanisms of achieving multi-Gbps backscatter with miniaturized RF front-ends and antennas in mmWave bands. An end-to-end system bandwidth of at least 4 GHz around 24 GHz has been achieved with off-the-shelf components and modules, demonstrating the extreme-datarate potential of picojoule-per-bit communicators. The performance has been verified with inkjet-printed fully-flexible front-ends and antenna arrays, which are directly compatible with wearable electronics for communication and sensing. We envision the full integration

978-1-5090-6360-4/17/$31.00 ©2017 IEEE

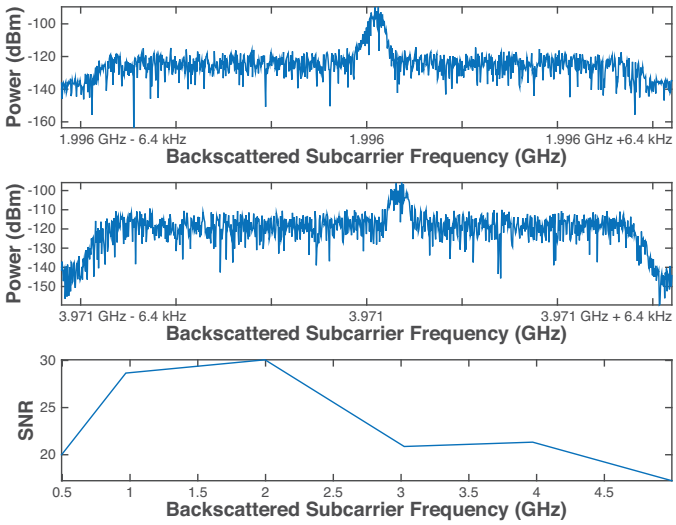

Fig. 5. Backscattered subcarrier at 2 GHz and 4 GHz, and SNR versus subcarrier frequency.

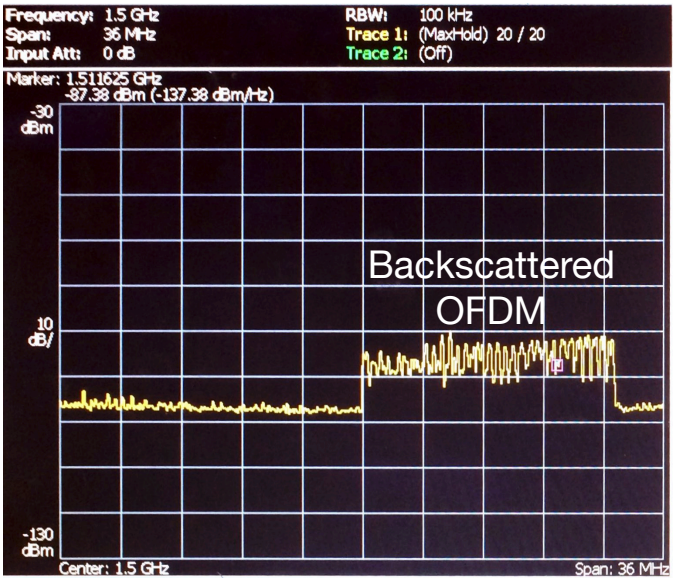

Fig. 6. Wideband backscatter OFDM signal spectrum.

of high-datarate, minimal-complexity, low-power backscatter front-ends with a high volume of mobile devices that will form dense 5G and IoT networks for mobile applications. Our future goals include the quantification of the broadband backscatter link performance under power, bandwidth, and interference constraints, as well as the optimization of the Tx/Rx chain and wideband signal processing to implement full receivers for multi-gigabit backscatter.

ACKNOWLEDGEMENTS

The work of J. Kimionis and M. M. Tentzeris was supported by the National Science Foundation-EFRI and the Defense Threat Reduction Agency (DTRA). The work of A. Georgiadis was supported under EU H2020 Marie Sklodowska-Curie Grant Agreement 661621 and EU COST Action IC1301 - Wireless Power Transmission for Sustainable Electronics.

REFERENCES

[1] V. Liu, A. Parks, V. Talla, S. Gollakota, D. Wetherall, and J. R. Smith, "Ambient Backscatter: Wireless Communication Out Of Thin Air," in *Proc. ACM SIGCOMM 2013 Conf. SIGCOMM*. Hong Kong, China: ACM, 2013, pp. 39–50.

[2] J. Kimionis, A. Bletsas, and J. N. Sahalos, "Increased range bistatic scatter radio," *IEEE Trans. Commun.*, vol. 62, no. 3, pp. 1091–1104, mar 2014.

[3] R. Correia, N. B. Carvalho, and S. Kawasaki, "Continuously Power Delivering for Passive Backscatter Wireless Sensor Networks," *IEEE Trans. Microw. Theory Tech.*, pp. 1–9, 2016.

[4] G. Vannucci, A. Bletsas, and D. Leigh, "A Software-Defined Radio System for Backscatter Sensor Networks," *IEEE Trans. Wirel. Commun.*, vol. 7, no. 6, pp. 2170–2179, jun 2008.

[5] P. Hu, P. Zhang, and D. Ganesan, "Laissez-Faire," in *Proc. 2015 ACM Conf. Spec. Interes. Gr. Data Commun. - SIGCOMM '15*, London, UK, 2015, pp. 255–267.

[6] S. J. Thomas, E. Wheeler, J. Teizer, and M. S. Reynolds, "Quadrature Amplitude Modulated Backscatter in Passive and Semipassive UHF RFID Systems," *IEEE Trans. Microw. Theory Tech.*, vol. 60, no. 4, pp. 1175–1182, apr 2012.

[7] J. Kimionis and M. M. Tentzeris, "Pulse Shaping: The Missing Piece of Backscatter Radio and RFID," *IEEE Trans. Microw. Theory Tech.*, vol. 64, no. 12, pp. 4774–4788, dec 2016.

[8] J. D. Griffin and G. D. Durgin, "Complete link budgets for backscatter-radio and RFID systems," *IEEE Antennas Propag. Mag.*, 2009.

[9] E. Kampianakis, J. Kimionis, K. Tountas, C. Konstantopoulos, E. Koutroulis, and A. Bletsas, "Wireless Environmental Sensor Networking With Analog Scatter Radio and Timer Principles," *IEEE Sens. J.*, vol. 14, no. 10, pp. 3365–3376, oct 2014.

978-1-5090-6360-4/17/$31.00 ©2017 IEEE